INTERNATIONAL JOURNAL FOR NUMERICAL METHODS IN FLUIDS
Int. J. Numer. Meth. Fluids 2008; **56**:257–277
Published online 15 May 2007 in Wiley InterScience (www.interscience.wiley.com). DOI: 10.1002/fld.1516

Görtler vortices in Falkner–Skan flows with suction and blowing

O. John E. Matsson*,†

Oral Roberts University, Engineering and Physics Department, 7777 South Lewis Ave., Tulsa, OK 74171-0001, U.S.A.

SUMMARY

In this paper, we use nonlinear calculations to study curved boundary-layer flows with pressure gradients and self-similar suction or blowing. For an accelerated outer flow, stabilization occurs in the linear region while the saturation amplitude of vortices is larger than for flows with a decelerating outer flow. The combined effects of boundary-layer suction and a favourable pressure gradient can give a significant stabilization of the flow. Streamwise vortices can be amplified on both concave and convex walls for decelerated Falkner–Skan flow with an overshoot in the velocity profile. The disturbance amplitude is generally lower far downstream compared with profiles without overshoot. Copyright © 2007 John Wiley & Sons, Ltd.

Received 17 October 2006; Revised 21 March 2007; Accepted 26 March 2007

KEY WORDS: Görtler vortices; Falkner–Skan flow; suction and blowing

1. INTRODUCTION

Solutions to the Falkner–Skan equation with an overshoot in the velocity profile have earlier been excluded in the boundary-layer literature as being physically unacceptable since the velocity should always be less than the freestream value, see Rosenhead [1]. However, Libby and Liu [2] argued that an initial length must be excluded in the solution of the Falkner–Skan equation for adverse pressure gradients. If the external flow is established beyond the initial length, the influence will decay further downstream and the similarity solution will describe the flow more accurately. Different branches of the solution to the Falkner–Skan equation for adverse pressure gradients can be related to different velocity profiles at the end of the initial length region.

The first branch for decelerated flow with an overshoot in the velocity profile was shown by Steinheuer [3], who interpreted the solution as a wall jet in a retarded outer flow, and it was shown that as the velocity gradient becomes infinite the solution of the Falkner–Skan equation approaches

*Correspondence to: O. John E. Matsson, Oral Roberts University, Engineering and Physics Department, 7777 South Lewis Ave., Tulsa, OK 74171-0001, U.S.A.
†E-mail: jmatsson@oru.edu

the wall jet without freestream as described by Glauert [4]. Libby and Liu have shown that there exists at least four branches for adverse pressure gradients and Zaturska and Banks [5] found a new branch related to favourable pressure gradients. Solutions to the Falkner–Skan equation in the form of overshoot velocity profiles have also been included in the textbooks by White [6] and Sobey [7].

Overshoot profiles are unstable on both concave and convex walls and streamwise vortices can develop. On curved walls the Görtler number is the appropriate parameter for the stability problem. The Görtler number is defined as $Go = Re\sqrt{\varepsilon}$, the curvature parameter $\varepsilon = \delta/R$, where R is the radius of curvature of the wall and $\delta = \sqrt{vx/U_\infty}$ is the boundary-layer thickness, where x is the streamwise coordinate and v is the kinematic viscosity. The Reynolds number is defined as $Re = U_\infty \delta/v$, where U_∞ is the freestream velocity. Streamwise vortices in curved boundary layers have been studied frequently both numerically and experimentally, for a review see Hall [8], Saric [9], and Floryan [10]. However, studies of streamwise vortices in wall jet flows are more sparse. The first parallel neutral stability calculations were made by Kahawita [11] for the Glauert wall jet without freestream. Non-parallel linear stability theory was used by Floryan [12, 13], followed by Matsson [14] who studied the influence of system rotation and self-similar suction or blowing on wall jets. Wadey [15] used asymptotic methods for linear theory to study Görtler vortices in wall jet flows for large spanwise wavenumbers. It was found that curved wall jets on both concave and convex walls were more stable to streamwise vortices than boundary-layer flows.

An experimental study of streamwise vortices appeared for wall jet flow on a concave wall, see Matsson [16], followed by nonlinear simulations of the same flow by Le Cunff and Zebib [17]. The simulations were able to capture the primary instability of streamwise vortices in the experiments. They also found that for low Görtler numbers the disturbance amplitude initially could be increased but the amplitude further downstream attained an amplitude which was lower than the starting level. However, at higher Görtler numbers the streamwise vortices increased exponentially in amplitude followed by a maximum and an almost constant level further downstream. The growth of streamwise vortices in wall jets on a convex wall has also been studied experimentally by Matsson [18]. Görtler vortices were triggered and the development was measured and visualized on a rotating cylinder.

The influence of pressure gradients on streamwise vortices in Blasius boundary-layer flows have been studied numerically by Ragab and Nayfeh [19], Goulpie *et al.* [20], Itoh [21], and experimentally by Aihara and Sonoda [22]. The results by Goulpie *et al.* were very sensitive to initial conditions and it was proposed that a definite answer could only be reached from receptivity studies. In the experimental study of Aihara and Sonoda the pressure was constant in the linear region followed by a favourable or adverse pressure gradient in the nonlinear region where the secondary instability appeared as a horseshoe mode of instability. A favourable pressure gradient reduced the boundary-layer thickness and the high shear regions near the boundary-layer edge which stabilized the flow and suppressed the secondary instability. An adverse pressure gradient increased the boundary-layer thickness and the high shear layer was moving further away from the wall.

The effects of suction and blowing on the Blasius boundary layer on concave walls have been studied by Floryan and Saric [23], Floryan [24] and Lin and Hwang [25]. It was found that the flow was stabilized for increased asymptotic suction and also shown that for self-similar suction the flow was destabilized for low spanwise wave numbers up to a certain value of suction and stabilized for even stronger suction. Moreover, the lowest critical Görtler number corresponded to the disappearance of the wall-normal velocity component at the boundary-layer edge.

DOI: 10.1002/fld

An experimental study by Myose and Blackwelder [26] used selective suction to control streamwise vortices in boundary layers. They used suction at single locations under the low-speed regions in order to get a fuller velocity profile and decrease the velocity gradients in the spanwise direction and thereby stabilize the flow. At a certain level of suction it was possible to stabilize the flow and move the transition region further downstream. The suction level to get stabilization was approximately two orders of magnitude lower than the corresponding level to achieve an asymptotic suction velocity profile. For high levels of suction the flow was destabilized which was related to an instability in the spanwise direction.

2. THEORY

The velocity vector $\overline{U}$ in a cylindrical coordinate system can be described as

$$\overline{U} = u_r \overline{e}_r + u_\varphi \overline{e}_\varphi + u_\zeta \overline{e}_\zeta \tag{1}$$

where u_r, u_φ, and u_ζ are the velocity components in the radial, streamwise, and spanwise directions, respectively. The momentum equations have the following form for a curved geometry:

$$\frac{Du_r}{Dt_d} - \frac{u_\varphi^2}{r} = -\frac{1}{\rho}\frac{\partial p_d}{\partial r} + \nu\left(\nabla^2 u_r - \frac{u_r}{r^2} - \frac{2}{r^2}\frac{\partial u_\varphi}{\partial \varphi}\right) \tag{2}$$

$$\frac{Du_\varphi}{Dt_d} + \frac{u_\varphi u_r}{r} = -\frac{1}{\rho r}\frac{\partial p_d}{\partial \varphi} + \nu\left(\nabla^2 u_\varphi - \frac{u_\varphi}{r^2} + \frac{2}{r^2}\frac{\partial u_r}{\partial \varphi}\right) \tag{3}$$

$$\frac{Du_\zeta}{Dt_d} = -\frac{1}{\rho}\frac{\partial p_d}{\partial \zeta} + \nu\nabla^2 u_\zeta \tag{4}$$

$$\frac{\partial u_r}{\partial r} + \frac{u_r}{r} + \frac{\partial u_\varphi}{r\partial \varphi} + \frac{\partial u_\zeta}{\partial \zeta} = 0 \tag{5}$$

where

$$\frac{D}{Dt_d} = \frac{\partial}{\partial t_d} + u_r\frac{\partial}{\partial r} + \frac{u_\varphi}{r}\frac{\partial}{\partial \varphi} + u_\zeta\frac{\partial}{\partial \zeta}, \quad \nabla^2 = \frac{1}{r}\frac{\partial}{\partial r}\left(r\frac{\partial}{\partial r}\right) + \frac{1}{r^2}\frac{\partial^2}{\partial \varphi^2} + \frac{\partial^2}{\partial \zeta^2} \tag{6}$$

We introduce the dimensionless coordinates x, y, z defined as

$$x = \frac{\varphi}{\varepsilon Re}, \quad y = \frac{(-1)^q (r - R)}{\delta}, \quad z = \frac{\zeta}{\delta} \tag{7}$$

where $q = 0, 1$ on convex and concave walls, respectively. The dimensionless velocities u_x, u_y, u_z and the pressure p are defined as

$$u_x = \frac{u_\varphi}{U_\infty}, \quad u_y = \frac{(-1)^q u_r Re}{U_\infty}, \quad u_z = \frac{u_\zeta Re}{U_\infty}, \quad p = \frac{p_d Re^2}{\rho U_\infty^2} \tag{8}$$

The velocity vector can be divided into mean-flow components in the streamwise and wall-normal directions plus a perturbation

$$\overline{U} = [U(x, y) + u]\overline{e}_x + [V(x, y) + v]\overline{e}_y + w\overline{e}_z \tag{9}$$

DOI: 10.1002/fld

A perturbation is introduced in the form

$$u, v, w, p = \sum_{n=-\infty}^{\infty} [u_n(x, y), v_n(x, y), w_n(x, y), p_n(x, y)]\mathrm{e}^{\mathrm{i}n\alpha z} \tag{10}$$

where α is the spanwise wave number and $u_n(x, y)$, $v_n(x, y)$, $w_n(x, y)$, and $p_n(x, y)$ are eigenfunctions. For large Reynolds number Re and small curvature parameter ε, Equations (1)–(4) can be written as

$$\left(n^2\alpha^2 + \frac{\partial(U + u_0)}{\partial x}\right) u_n + (U + u_0)\frac{\partial u_n}{\partial x} + (V + v_0)\frac{\partial u_n}{\partial y} = \frac{\partial^2 u_n}{\partial y^2} - \frac{\partial(U + u_0)}{\partial y} v_n \tag{11}$$

$$\left(n^2\alpha^2 + \frac{\partial(V + v_0)}{\partial y}\right) v_n + (U + u_0)\frac{\partial v_n}{\partial x} + (V + v_0)\frac{\partial v_n}{\partial y}$$

$$= -\frac{\partial p_n}{\partial y} + \frac{\partial^2 v_n}{\partial y^2} + \left(2(-1)^q Go^2(U + u_0) - \frac{\partial(V + v_0)}{\partial x}\right) u_n \tag{12}$$

$$n^2\alpha^2 w_n + (U + u_0)\frac{\partial w_n}{\partial x} + (V + v_0)\frac{\partial w_n}{\partial y} = -\mathrm{i}n\alpha p_n + \frac{\partial^2 w_n}{\partial y^2} \tag{13}$$

$$\frac{\partial u_n}{\partial x} + \frac{\partial v_n}{\partial y} + \mathrm{i}n\alpha w_n = 0 \tag{14}$$

where we have collected terms multiplied with the same exponential function. The boundary conditions for the different Fourier modes $n \neq 0$ are

$$u_n, v_n, w_n = 0 \text{ at } y = 0 \quad \text{and} \quad u_n, v_n, w_n \to 0 \text{ as } y \to \infty \tag{15}$$

The boundary conditions for mean-flow distortion $n = 0$

$$u_0, v_0, w_0 = 0 \text{ at } y = 0 \quad \text{and} \quad u_0, w_0 \to 0 \text{ as } y \to \infty \tag{16}$$

and the component v_0 must be evaluated by integration

$$v_0(x, y) = -\int_0^y \frac{\partial u_0}{\partial x}(x, s)\,\mathrm{d}s \tag{17}$$

The basic flow velocity components can be expressed in terms of a streamfunction

$$\Psi(\xi, \eta) = (f(\eta) - 2\gamma)\xi^{(1+m)/(1-m)} \tag{18}$$

as

$$U = \frac{\partial \Psi}{\partial y}, \quad V = -\frac{\partial \Psi}{\partial x} \tag{19}$$

DOI: 10.1002/fld

where $\eta = y/\xi$, $\xi = x^{(1-m)/2}$, γ is the suction/blowing parameter and m is related to the pressure gradient parameter $\beta = 2m/(m+1)$. The basic flow quantities are given by

$$U = f'(\eta)\xi^{2m/(1-m)}, \quad V = \frac{-(1+m)f(\eta) + (1-m)\eta f'(\eta) + 2\gamma(1+m)}{2\xi} \tag{20}$$

$$U_x = \frac{2m f'(\eta) - (1-m)\eta f''(\eta)}{2\xi^2}, \quad U_y = f'''(\eta)\xi^{(1-3m)/(m-1)} \tag{21}$$

$$V_x = (1-m)[(1+m)f(\eta) - (1-3m)\eta f'(\eta) - (1-m)\eta^2 f''(\eta)]\xi^{(3-m)/(m-1)} \tag{22}$$

$$V_y = \frac{-2m f'(\eta) + (1-m)\eta f''(\eta)}{2\xi^2} \tag{23}$$

and the equation for $f(\eta)$ is

$$f'''(\eta) + 0.5(1+m)f(\eta)f''(\eta) + m[1 - f'(\eta)^2] - (1+m)\gamma f''(\eta) = 0 \tag{24}$$

Using Equations (13) and (14), we eliminate the pressure from Equation (12). Equations (11) and (12) can then be written as

$$\left(n^2\alpha^2 + \frac{\partial U}{\partial x}\right)u_n + U\frac{\partial u_n}{\partial x} + V\frac{\partial u_n}{\partial y} - \frac{\partial^2 u_n}{\partial y^2} + \frac{\partial U}{\partial y}v_n = No_{1n}(x, y) \tag{25}$$

$$\begin{aligned} &- \left(n^4\alpha^4 + n^2\alpha^2\frac{\partial V}{\partial y} + \frac{\partial^3 U}{\partial x \partial y^2}\right)v_n - \left(n^2\alpha^2 U + \frac{\partial^2 U}{\partial y^2}\right)\frac{\partial v_n}{\partial x} \\ &+ U\frac{\partial^3 v_n}{\partial x \partial y^2} - \left(n^2\alpha^2 V + \frac{\partial^2 U}{\partial x \partial y}\right)\frac{\partial v_n}{\partial y} \\ &+ \left(2n^2\alpha^2 + \frac{\partial V}{\partial y}\right)\frac{\partial^2 v_n}{\partial y^2} + V\frac{\partial^3 v_n}{\partial y^3} - \frac{\partial^4 v_n}{\partial y^4} \\ &+ \left(n^2\alpha^2\left(2(-1)^q Go^2 U - \frac{\partial V}{\partial x}\right) - \frac{\partial^3 U}{\partial x^2 \partial y}\right) \\ &\times u_n - 2\frac{\partial^2 U}{\partial x \partial y}\frac{\partial u_n}{\partial x} - 2\frac{\partial U}{\partial x}\frac{\partial^2 u_n}{\partial x \partial y} - \frac{\partial V}{\partial x}\frac{\partial^2 u_n}{\partial y^2} = No_{2n}(x, y) \end{aligned} \tag{26}$$

The coordinates x and y are transformed into the boundary-layer coordinates ξ and η, and by substituting the basic flow velocity components and their derivatives in Equations (25)–(26)

DOI: 10.1002/fld

we get the following coupled equations:

$$2\frac{\partial^2 u_n}{\partial\eta^2} + ((1+m)f - 2(1+m)\gamma)\frac{\partial u_n}{\partial\eta} - (1-m)\xi\frac{\mathrm{d}f}{\mathrm{d}\eta}\frac{\partial u_n}{\partial\xi} + \left((1-m)\eta\frac{\mathrm{d}^2 f}{\mathrm{d}\eta^2} + 2m\frac{\mathrm{d}f}{\mathrm{d}\eta} - 2n^2\alpha^2\xi^2\right)u_n - 2\xi^{(1+m)/(1-m)}\frac{\mathrm{d}^2 f}{\mathrm{d}\eta^2}v_n = -2\xi^2 No_{1n}(\xi,\eta) \tag{27}$$

$$\begin{aligned}
&4\xi\frac{\partial^4 v_n}{\partial\eta^4} + 2(1+m)\xi(f-2\gamma)\frac{\partial^3 v_n}{\partial\eta^3} + \left(4\xi\frac{\mathrm{d}f}{\mathrm{d}\eta} - 2(1-m)\xi\eta\frac{\mathrm{d}^2 f}{\mathrm{d}\eta^2} - 8n^2\alpha^2\xi^3\right)\frac{\partial^2 v_n}{\partial\eta^2}\\
&- \left(4(1-m)\xi\eta\frac{\mathrm{d}^3 f}{\mathrm{d}\eta^3} + 2(1-3m)\xi\frac{\mathrm{d}^2 f}{\mathrm{d}\eta^2} + 2(1+m)n^2\alpha^2\xi^3(f-2\gamma)\right)\frac{\partial v_n}{\partial\eta}\\
&+ \left[2(m-1)\xi\eta\frac{\mathrm{d}^4 f}{\mathrm{d}\eta^4} - (4-8m)\xi\frac{\mathrm{d}^3 f}{\mathrm{d}\eta^3} + 2n^2\alpha^2\xi^3\left((1-m)\eta\frac{\mathrm{d}^2 f}{\mathrm{d}\eta^2} - 2m\frac{\mathrm{d}f}{\mathrm{d}\eta}\right) + 4n^4\alpha^4\xi^5\right]v_n\\
&+ \left[\xi^{2m/(m-1)}\left((m-1)^2\eta^2\frac{\mathrm{d}^4 f}{\mathrm{d}\eta^4} + (5-12m+7m^2)\eta\frac{\mathrm{d}^3 f}{\mathrm{d}\eta^3} + 3(1-4m+3m^2)\frac{\mathrm{d}^2 f}{\mathrm{d}\eta^2}\right.\right.\\
&+ n^2\alpha^2\xi^2\left((1-m^2)f - (1-4m+3m^2)\eta\frac{\mathrm{d}f}{\mathrm{d}\eta} - (m-1)^2\eta^2\frac{\mathrm{d}^2 f}{\mathrm{d}\eta^2} - 2\gamma(1-m^2)\right)\\
&\left.\left. - 8(-1)^q n^2\alpha^2 Go^2\xi^{(3m-5)/(m-1)}\frac{\mathrm{d}f}{\mathrm{d}\eta}\right]u_n + 2(1-m)\left(\xi^2\frac{\mathrm{d}^3 f}{\mathrm{d}\eta^3} + n^2\alpha^2\xi^4\frac{\mathrm{d}f}{\mathrm{d}\eta}\right)\frac{\partial v_n}{\partial\xi}\right.\\
&- 2(1-m)\xi^2\frac{\mathrm{d}f}{\mathrm{d}\eta}\frac{\partial^3 v_n}{\partial\xi\partial\eta^2} - 2\xi^{(3m-1)/(m-1)}\left((m-1)^2\eta\frac{\mathrm{d}^3 f}{\mathrm{d}\eta^3} + (1-4m+3m^2)\frac{\mathrm{d}^2 f}{\mathrm{d}\eta^2}\right)\frac{\partial u_n}{\partial\xi}\\
&+ \xi^{2m/(m-1)}\left(2(m-1)^2\eta^2\frac{\mathrm{d}^3 f}{\mathrm{d}\eta^3} + 4(1-3m+2m^2)\eta\frac{\mathrm{d}^2 f}{\mathrm{d}\eta^2} - 4m(1-m)\frac{\mathrm{d}f}{\mathrm{d}\eta}\right)\frac{\partial u_n}{\partial\eta}\\
&- 2\xi^{(3m-1)/(m-1)}\left((m-1)^2\eta\frac{\mathrm{d}^2 f}{\mathrm{d}\eta^2} - 2m(1-m)\frac{\mathrm{d}f}{\mathrm{d}\eta}\right)\frac{\partial^2 u_n}{\partial\xi\partial\eta}\\
&+ \xi^{2m/(m-1)}\left((m-1)^2\eta^2\frac{\mathrm{d}^2 f}{\mathrm{d}\eta^2} - (1-m^2)\left(\eta\frac{\mathrm{d}f}{\mathrm{d}\eta} - f + 2\gamma\right)\right)\frac{\partial^2 u_n}{\partial\eta^2} = 4\xi^5 No_{2n}(\xi,\eta)
\end{aligned} \tag{28}$$

where No_{1n} and No_{2n} are Fourier coefficients of the nonlinear terms. For a more complete derivation of the nonlinear terms without pressure gradient and suction/blowing, see Benmalek [27].

DOI: 10.1002/fld

3. DISCRETIZATION AND NUMERICAL SOLUTION PROCEDURE

Equations (27)–(28) are solved in a similar manner as by Benmalek and Saric [28] with a second-order central difference scheme in the wall-normal direction and with a second-order backward difference scheme in the the streamwise direction which gives the following discretized equations:

$$\begin{aligned} &a_{1k}^{j+1}u_{n,k+1}^{j+1,M+1}+a_{2k}^{j+1}u_{n,k}^{j+1,M+1}+a_{3k}^{j+1}u_{n,k-1}^{j+1,M+1}\\ &\quad=b_{1k}^{j+1}u_{n,k+1}^{j+1,M}+b_{2k}^{j+1}u_{n,k}^{j+1,M}+b_{3k}^{j+1}u_{n,k-1}^{j+1,M}+b_{4k}^{j+1}v_{n,k}^{j+1,M}\\ &\qquad+b_{5k}^{j+1}u_{n,k}^{j}+b_{6k}^{j+1}u_{n,k}^{j-1}+2\xi_{j+1}^{2}(No_{1n})_{k}^{j+1,M} \end{aligned} \tag{29}$$

$$\begin{aligned} &c_{1k}^{j+1}v_{n,k+2}^{j+1,M+1}+c_{2k}^{j+1}v_{n,k+1}^{j+1,M+1}+c_{3k}^{j+1}v_{n,k}^{j+1,M+1}+c_{4k}^{j+1}v_{n,k-1}^{j+1,M+1}+c_{5k}^{j+1}v_{n,k-2}^{j+1,M+1}\\ &\quad=d_{1k}^{j+1}v_{n,k+2}^{j+1,M}+d_{2k}^{j+1}v_{n,k+1}^{j+1,M}+d_{3k}^{j+1}v_{n,k}^{j+1,M}+d_{4k}^{j+1}v_{n,k-1}^{j+1,M}+d_{5k}^{j+1}v_{n,k-2}^{j+1,M}\\ &\qquad+d_{6k}^{j+1}u_{n,k+1}^{j+1,M+1}+d_{7k}^{j+1}u_{n,k}^{j+1,M+1}+d_{8k}^{j+1}u_{n,k-1}^{j+1,M+1}+d_{9k}^{j+1}u_{n,k+1}^{j}+d_{10k}^{j+1}u_{n,k}^{j}+d_{11k}^{j+1}u_{n,k-1}^{j}\\ &\qquad+d_{12k}^{j+1}v_{n,k-1}^{j}+d_{13k}^{j+1}v_{n,k}^{j}+d_{14k}^{j+1}v_{n,k+1}^{j}+d_{15k}^{j+1}v_{n,k-1}^{j-1}+d_{16k}^{j+1}v_{n,k}^{j-1}+d_{17k}^{j+1}v_{n,k+1}^{j-1}\\ &\qquad+d_{18k}^{j+1}u_{n,k+1}^{j-1}+d_{19k}^{j+1}u_{n,k}^{j-1}+d_{20k}^{j+1}u_{n,k-1}^{j-1}+4\xi_{j+1}^{5}(No_{2n})_{k}^{j+1,M} \end{aligned} \tag{30}$$

After discretization of Equations (14) and (17) we get

$$\begin{aligned} g_{1k}^{j+1}w_{n,k}^{j+1,M+1}&=h_{1k}^{j+1}u_{n,k+1}^{j+1,M+1}+h_{2k}^{j+1}u_{n,k}^{j+1,M+1}+h_{3k}^{j+1}u_{n,k-1}^{j+1,M+1}\\ &\quad+h_{4k}^{j+1}u_{n,k}^{j}+h_{5k}^{j+1}u_{n,k}^{j-1}+h_{6k}^{j+1}v_{n,k+1}^{j+1,M+1}+h_{7k}^{j+1}v_{n,k-1}^{j+1,M+1} \end{aligned} \tag{31}$$

$$v_{0,k}^{j+1,M+1}=-\frac{(1-m)}{2\xi_{j+1}^{2/(1-m)}}\int_{0}^{\eta_k}\left(\xi\frac{\partial u_0}{\partial\xi}-\eta\frac{\partial u_0}{\partial\eta}\right)_{j+1}\mathrm{d}\eta \tag{32}$$

where the coefficients of Equations (29)–(31) are given in the Appendix. M is an iteration number and the streamwise position is given by $\xi_j=1+j\Delta\xi$ where $j\geqslant 1$. The streamwise step in the calculations was chosen in the region $\Delta\xi=0.01-0.05$ depending on the pressure gradient. For smaller values of the pressure gradient, a larger value of the streamwise step would give convergence of the numerical scheme. The wall-normal position is defined as $\eta_k=k\Delta\eta$, where $1\leqslant k\leqslant K$. The wall-normal step was $\Delta\eta=0.1$ and $K=200$ points were included in this direction. Eight modes ($0\leqslant n\leqslant N$) were included in the nonlinear calculations. In the nonlinear region an under-relaxation factor was included in order to get convergence. The tolerance in the convergence condition for all velocity components was as low as 10^{-14} in the linear region but increased when the linear and nonlinear terms were of the same order of magnitude. The tolerance, step sizes, number of modes, and number of points in the wall-normal direction were chosen to ensure convergence for

DOI: 10.1002/fld

Table I. Grid size test for $Go=2$, $\alpha=0.22$, $m=\gamma=0$ and $q=1$.

		x				
$\Delta\xi$	$\Delta\eta$	3	6	9	12	15
0.005	0.05	0.01585	0.04342	0.1589	0.3059	0.2568
0.005	0.1	0.01587	0.04356	0.1592	0.3073	0.2575
0.01	0.05	0.01585	0.04345	0.1591	0.3059	0.2568
0.01	0.1	0.01588	0.04360	0.1593	0.3073	0.2575

all modes, obtain accurate solutions, and limit the computational costs. The procedure to solve the velocity field consists of the following:

(a) Start the iterations by computing

$$u_{n,k}^{j+1,M}=2u_{n,k}^{j}-u_{n,k}^{j-1},\ v_{n,k}^{j+1,M}=2v_{n,k}^{j}-v_{n,k}^{j-1},\ w_{n,k}^{j+1,M}=2w_{n,k}^{j}-w_{n,k}^{j-1} \tag{33}$$

followed by the use of Equation (29) to determine $u_{n,k}^{j+1,M+1}$.

(b) Evaluate $v_{0,k}^{j+1,M+1}$ and $v_{n,k}^{j+1,M+1}$ using Equations (32) and (30), respectively.

(c) Equation (31) is used to determine $w_{n,k}^{j+1,M+1}$.

(d) Repeat the process until the absolute values of $u_{n,k}^{j+1,M+1}-u_{n,k}^{j+1,M}$, $v_{n,k}^{j+1,M+1}-v_{n,k}^{j+1,M}$, $w_{n,k}^{j+1,M+1}-w_{n,k}^{j+1,M}$ are smaller than the tolerance level.

For the numerical checks we studied the solution for $\eta_\infty=20$ and eight modes at various streamwise positions, see Table I, as the step sizes $\Delta\xi$ and $\Delta\eta$ were varied. The table shows the maximum values of the streamwise disturbance velocity u'/U_∞ at different x positions.

4. CALCULATIONS OF THE BASIC FLOW

Several methods can be used to control the development of streamwise vortices on curved walls. Control of such vortices in wall-bounded flows can be achieved by, for example, system rotation, suction/blowing, heating/cooling, different curvature distributions or a streamwise pressure gradient. In this study we concentrate on suction/blowing and pressure gradients. For the calculations of the basic flow we choose to solve the Falkner–Skan equation numerically utilizing an iterative method. Interestingly, a non-iterative approach have been used by Liao [29] to solve this equation.

Figure 1(a) shows the velocity gradient at the wall of the streamwise velocity component for different values of the pressure gradient m (full lines) or for different values of the suction/blowing parameter γ (dashed line). Five branches are shown in Figure 1(a) related to the pressure gradient. For branch 1 separation occurs at $m=-0.09$. There is no overshoot of the velocity profile for branch 1 and branch 2 has one overshoot but no backflow as shown by Steinheuer [3]. The flow related to branch 2 separates at approximately $m=-0.4$. For branches 2–5 the Falkner–Skan equation can have two solutions for certain values of the pressure gradient. For $m=-0.4$ on branch 2 there is one velocity profile with $f''(0)=0.32$ and another with $f''(0)=0.97$. Moreover,

DOI: 10.1002/fld

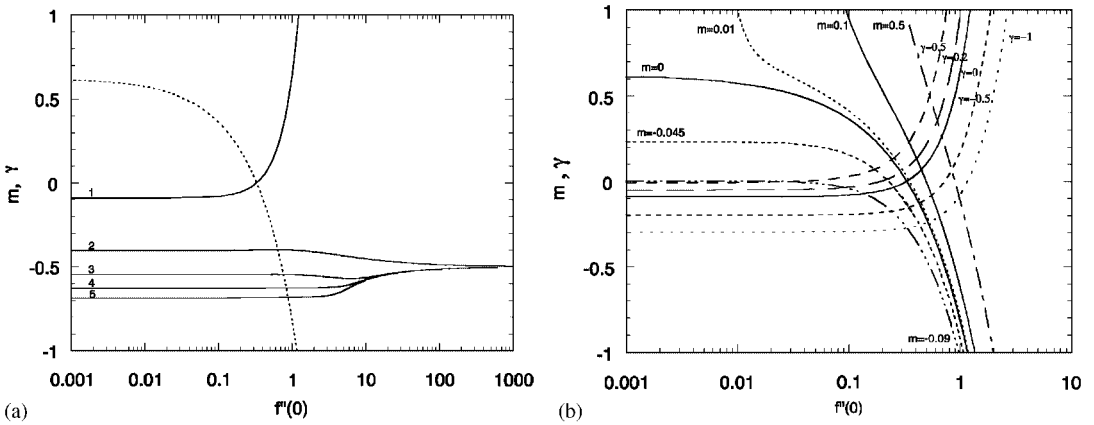

Figure 1. Streamwise velocity gradient at the wall $f''(0)$: (a) different values of the pressure gradient m (full lines) or suction/blowing γ (dashed line) and (b) combined pressure gradient m and suction/blowing γ.

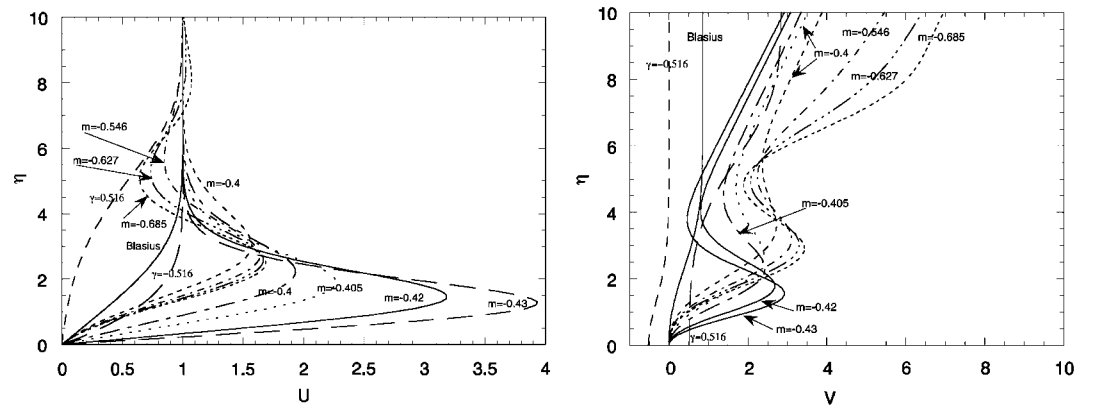

Figure 2. Profiles of the basic flow velocity components for different values of the pressure gradient m or the suction/blowing parameter γ.

the velocity gradient at the wall is very sensitive to a small change of the pressure gradient. Branches 3–5 are the same as shown by White [6]. However, in Figure 1(a) it is also shown that branches 3–5 approaches Glauerts wall jet solution with $m = 0.5$, corresponding to $\beta = -2$. Only one branch was found for suction without pressure gradient. For the value $\gamma = 0.61$ the velocity profile separates. In Figure 1(b) are the combined effects of both a pressure gradient and self-similar suction or blowing shown for branch 1. For suction the separating velocity profile appears at lower values of the pressure gradient than $m = -0.09$ without suction. For a pressure gradient larger than approximately $m = 0.01$ the basic flow was found not to separate at any value of the suction/blowing parameter.

The velocity profiles of the streamwise and wall-normal velocity components are shown in Figure 2 that shows some profiles of the basic flow at streamwise position $x = 1$ for different values

DOI: 10.1002/fld

of the suction parameter and the pressure gradient. One profile is shown for suction ($\gamma = -0.516$) and one profile for blowing ($\gamma = 0.516$). Overshoot velocity profiles are shown for different values of the pressure gradient.

5. NONLINEAR CALCULATIONS OF FLOWS WITHOUT VELOCITY OVERSHOOT

The stability equations require an initial condition at a streamwise position $x_0 = \varphi_0/\varepsilon Re = \varphi_0 R/\delta Re = x_0^*/L$ with the length scale L chosen as $L = x_0^*$. The nonlinear calculations were started at the streamwise position $x_0 = 1$ with a disturbance of the following form:

$$u_{01} = y^6 \mathrm{e}^{-y^2/2}, \quad v_{01} = 0 \tag{34}$$

Most calculations were made at $Go = 2$ and $\alpha = 0.22$ but also some calculations are included for a higher spanwise wave number $\alpha = 0.52$. A measure of the strength of vortices at a certain streamwise position is the integrated disturbance velocity of the streamwise velocity component

$$e = \left(\frac{1}{A} \int u'^2 \, \mathrm{d}A \right)^{0.5} \tag{35}$$

$$u'(y, z) = u(y, z) - \frac{1}{\lambda} \int u(y, z) \, \mathrm{d}z \tag{36}$$

where A was the cross-sectional area of integration, and $\lambda = 2\pi/\alpha$ is the spanwise wavelength. The same integrated disturbance amplitude $e = 0.005$ at $x = 1$ was chosen for all calculations. Figure 3 shows the streamwise development of Görtler vortices in curved Blasius boundary-layer flow ($\alpha = 0.22$) with self-similar suction or blowing. It is seen that blowing ($\gamma = 0.5164$, left column) increases the boundary-layer thickness and that suction ($\gamma = -0.5164$, right column) decreases the thickness compared with no suction or blowing (middle column). The mushroom structure appears clearly in the contour plots of the streamwise velocity component. In the lower part of Figure 3, contourplots are shown of the streamwise disturbance velocity, $u'(y, z)$, i.e. the streamwise velocity minus the spanwise averaged streamwise velocity profile. Positive (full lines) and negative (dashed lines) disturbance regions appear in the spanwise direction. As the flows develop in the nonlinear region two peaks appear in the wall-normal direction for both positive and negative disturbance regions. One peak is located near the wall at approximately $\eta = 1$ for all streamwise positions studied in the nonlinear flow region. The other peak is moving away from the wall as the mushroom structure becomes larger further downstream.

From the comparison in Figure 3 for different values of the suction/blowing parameter γ, only the velocity profile is affected by different γ but not the similarity coordinate η. However, when we compare contourplots for different values of the streamwise pressure gradient, the similarity coordinate is dependent on the pressure gradient and therefore the wall-normal coordinate y is used in the contourplots. Figure 4 shows ($\alpha = 0.22$) a comparison between the flow without pressure gradient in the middle column and a favourable and an adverse pressure gradient in the left and right columns, respectively. A favourable pressure gradient is seen to decrease the boundary-layer thickness and stabilize the flow for all streamwise positions. The boundary-layer thickness is increasing for an adverse pressure gradient and the vortices become wider in the spanwise direction.

DOI: 10.1002/fld

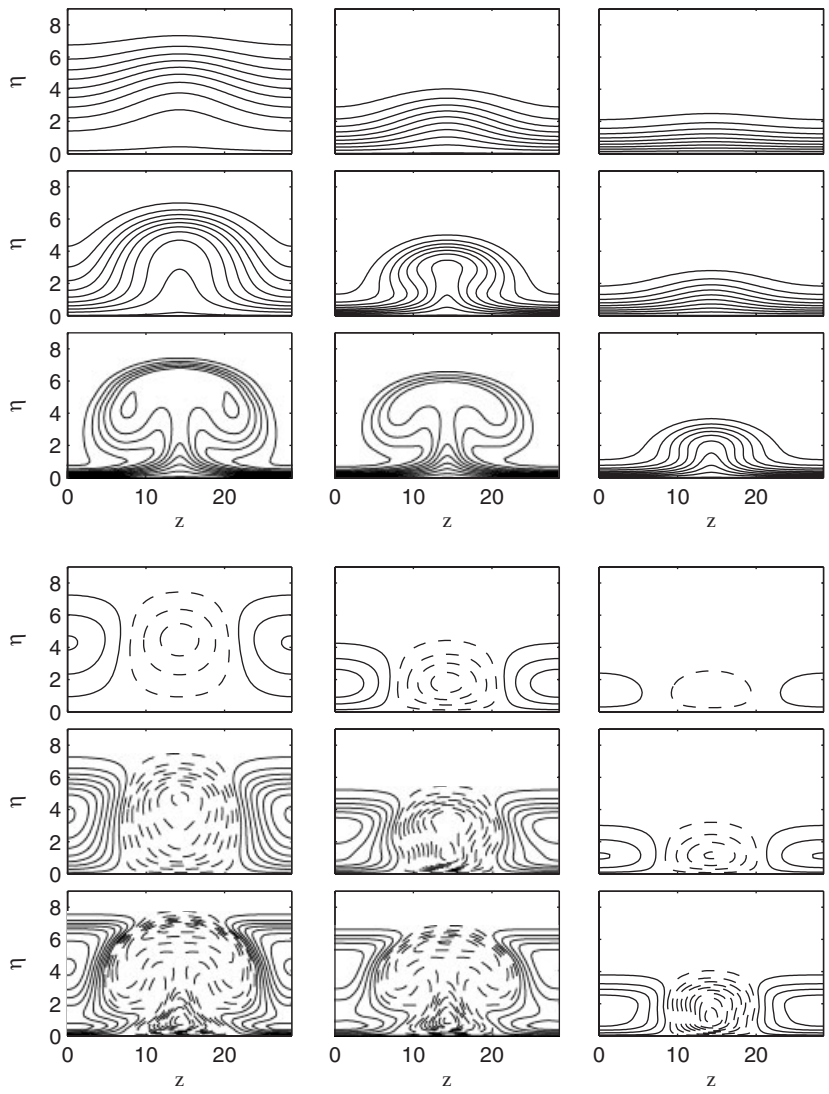

Figure 3. Streamwise velocity and disturbance velocity for $Go = 2$, $\alpha = 0.22$ on concave wall. Left column (blowing $\gamma = 0.516$), middle column ($\gamma = 0$), right column (suction $\gamma = -0.516$). Three different streamwise positions are shown increasing downwards ($x = 9$, 12, and 15), upper part: contour increment $0.1U_\infty$; lower part: contour increment $0.05U_\infty$.

Figure 5(a) shows the streamwise development of the disturbance amplitude e for streamwise velocity profiles with suction or blowing. Streamwise vortices in the Blasius boundary layer ($\gamma = 0$, $\alpha = 0.22$, full line) show an exponential growth in the linear region, followed by a maximum disturbance level in the nonlinear region and at streamwise positions further downstream the disturbance amplitude saturates at an almost constant level. The peak in the disturbance amplitude

DOI: 10.1002/fld

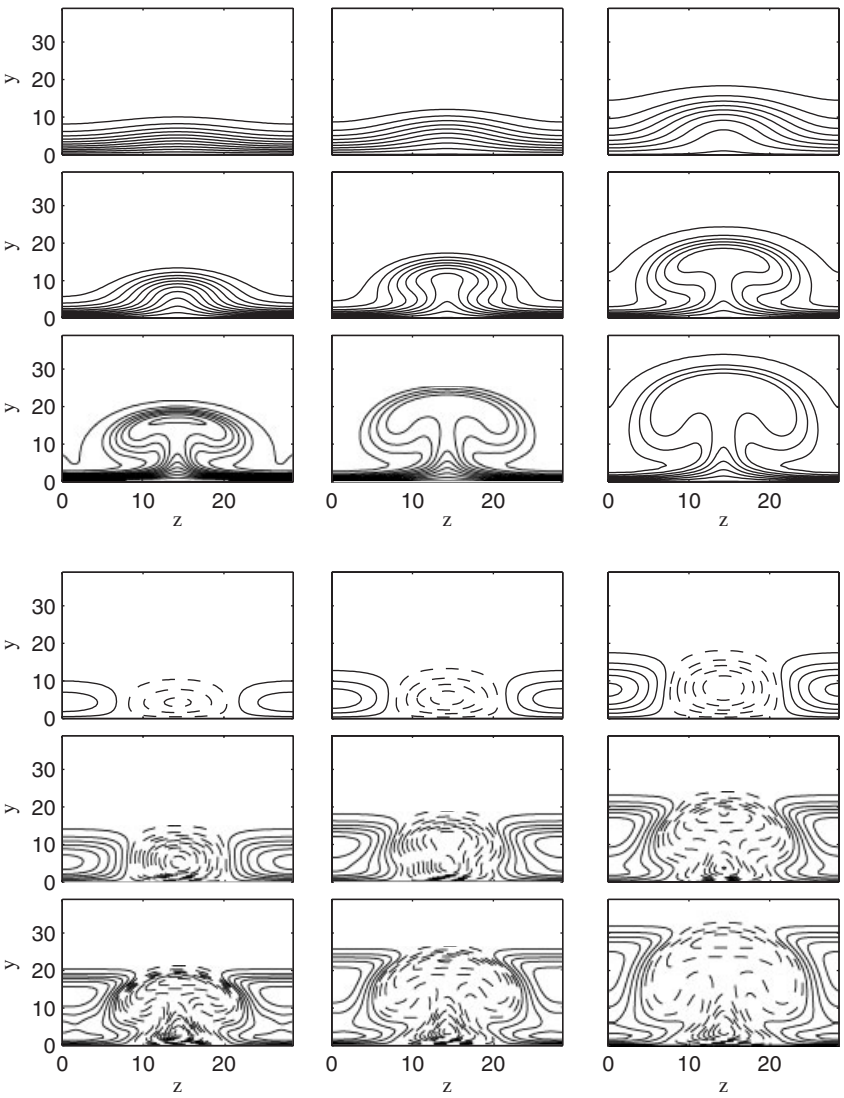

Figure 4. Streamwise velocity and disturbance velocity for $Go = 2$, $\alpha = 0.22$ on concave wall. Left column (favourable pressure gradient $m = 0.75$), middle column ($m = 0$), and right column (adverse pressure gradient $m = -0.075$). The same streamwise positions as in Figure 3 are shown.

has moved further upstream and has a higher level for $\gamma = 0.5164$ compared with no blowing. For suction the peak is positioned further downstream and the maximum level is lower than for blowing or no blowing/suction. For the higher spanwise wave number $\alpha = 0.52$ (dashed line) the growth in the linear region is smaller than for the lower wave number. The maximum amplitude of streamwise vortices appears slightly downstream and with a lower level compared with $\alpha = 0.22$. Moreover, the peak is not as pronounced as for the lower wave number. For suction $\gamma = -0.5164$,

DOI: 10.1002/fld

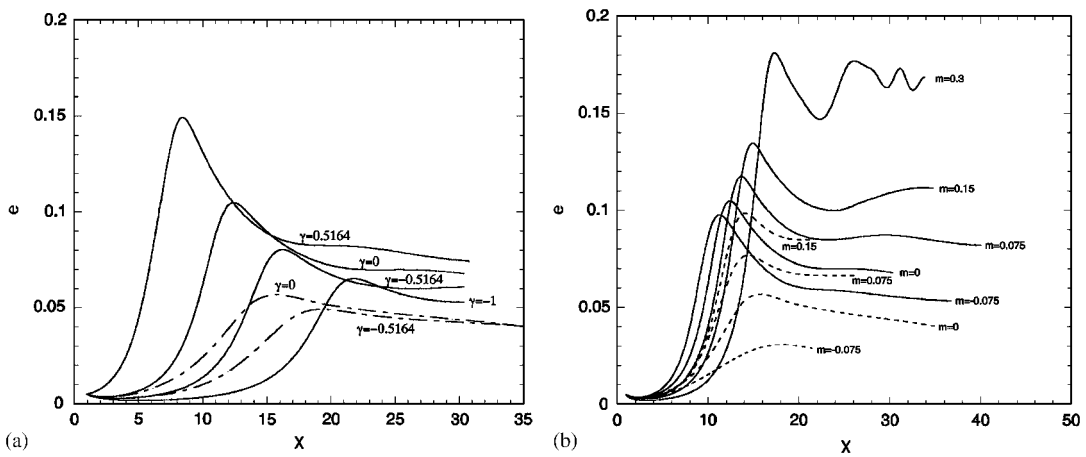

Figure 5. Integrated disturbance velocity e on a concave wall for $Go = 2$: (a) different suction/blowing γ and (b) different pressure gradient m (full lines $\alpha = 0.22$, dashed lines $\alpha = 0.52$).

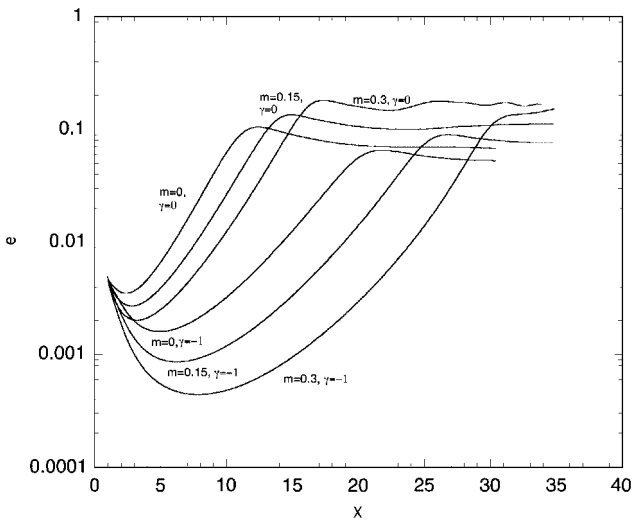

Figure 6. Streamwise development for $\alpha = 0.22$ of integrated disturbance velocity e on a concave wall for combined effects of suction/blowing γ and streamwise pressure gradient m.

the flow is also stabilized for this wave number but the amplitude approaches the level without suction far downstream.

A favourable streamwise pressure gradient ($m = 0.075$ and $\alpha = 0.22$ in Figure 5(b)) gives an accelerated outer flow which is seen to stabilize the flow in the linear region compared to $m = 0$. However, at streamwise positions downstream of $x = 12$, the strength of vortices is larger than the flow without a pressure gradient. For higher values of the favourable pressure gradient, $m = 0.15$ and $m = 0.3$ the flow is even more stabilized in the linear region but very unstable in the nonlinear region.

DOI: 10.1002/fld

At $m=0.3$, the integrated disturbance amplitude is not constant far downstream but is oscillating at an amplitude which is more than double the one without pressure gradient. Correspondingly, for an adverse pressure gradient ($m=-0.075$) the flow is destabilized in the initial growth region but the vortices saturate further downstream at an amplitude which is lower than both the Blasius boundary layer and the flow with a favourable pressure gradient. For the higher spanwise wavenumber $\alpha=0.52$ (dashed lines), the maximum amplitude is moving upstream as the pressure gradient is increasing, which is the opposite behaviour compared with the lower wave number.

The combined effects of both suction and a positive pressure gradient is shown in Figure 6 for $\alpha=0.22$. A substantial stabilization of the flow was achieved for $\gamma=-1$ and $m=0.15, 0.3$ compared with the other flow conditions shown in the figure. For the most stable flow shown ($\gamma=-1$ and $m=0.3$) the amplitude is decreasing at the start of curvature to a value which is more than one order of magnitude lower than the starting amplitude at $x=1$. The minimum amplitude appears at $x=8$ followed by growth of vortices and at $x=22$ the strength of vortices is the same as it was at the starting position. Further downstream the amplitude is growing and approaches the amplitude level for the case $m=0.3$.

6. NONLINEAR CALCULATIONS OF FLOWS WITH VELOCITY OVERSHOOT

In this section contourplots of the streamwise velocity and streamwise disturbance velocity will be shown followed by the streamwise development of vortex amplitude for solutions of the Falkner–Skan equation with velocity overshoot.

Contourplots are shown in Figure 7 for the wall jet in a freestream along branch 2 for three different streamwise velocity gradients at the wall. At $x=9$ the vortices are weak for ($m=-0.4$, $f''(0)=0.97$) as shown in the middle column and in the column on the right side ($m=-0.405$), but for the left column ($m=-0.4$, $f''(0)=0.32$) the vortices are stronger and the wall jet extends a little bit further out from the wall than for the other two cases. In comparison with velocity profiles without overshoot, the mushroom structure cannot persist as far downstream as for flows without overshoot. In the contourplot of the disturbance velocity there are perturbation regions in the outer part of the velocity profile that were absent for flows without overshoot.

From the contourplot of the disturbance velocity in the left column it is seen that the inflow region from the concave wall is splitting into two regions in the wall-normal direction as the flow develops downstream between $x=9$ and 12. Even further downstream at $x=15$, the outer negative disturbance region has disappeared. A similar behaviour was observed between $x=12$ and 15 for positive disturbance regions near the wall. At $x=15$ the disturbance regions for the left column ($m=-0.4$, $f''(0)=0.32$) have approximately the same wall-normal extension as at $x=9$. For the other velocity profile $f''(0)=0.97$ (middle column) and the same pressure gradient ($m=-0.4$) as for the left column, the flow behaviour is the same but the growth of vortices is lower and for $m=-0.405$ in the right column the streamwise growth is lower compared with the other two cases.

In Figure 8 are contourplots shown on the streamwise development of Görtler vortices for overshoot profiles along branch 3 (left column $m=-0.546$), branch 4 (middle column $m=-0.627$), and branch 5 (right column $m=-0.685$). For an increasing branch number the wall jet with freestream is becoming wider in the wall-normal direction due to a larger number of overshoots from the streamwise velocity profile. For the wall jet-type profiles the mushroom structures cannot develop freely in the wall-normal direction due to the shape of the velocity profile. The

DOI: 10.1002/fld

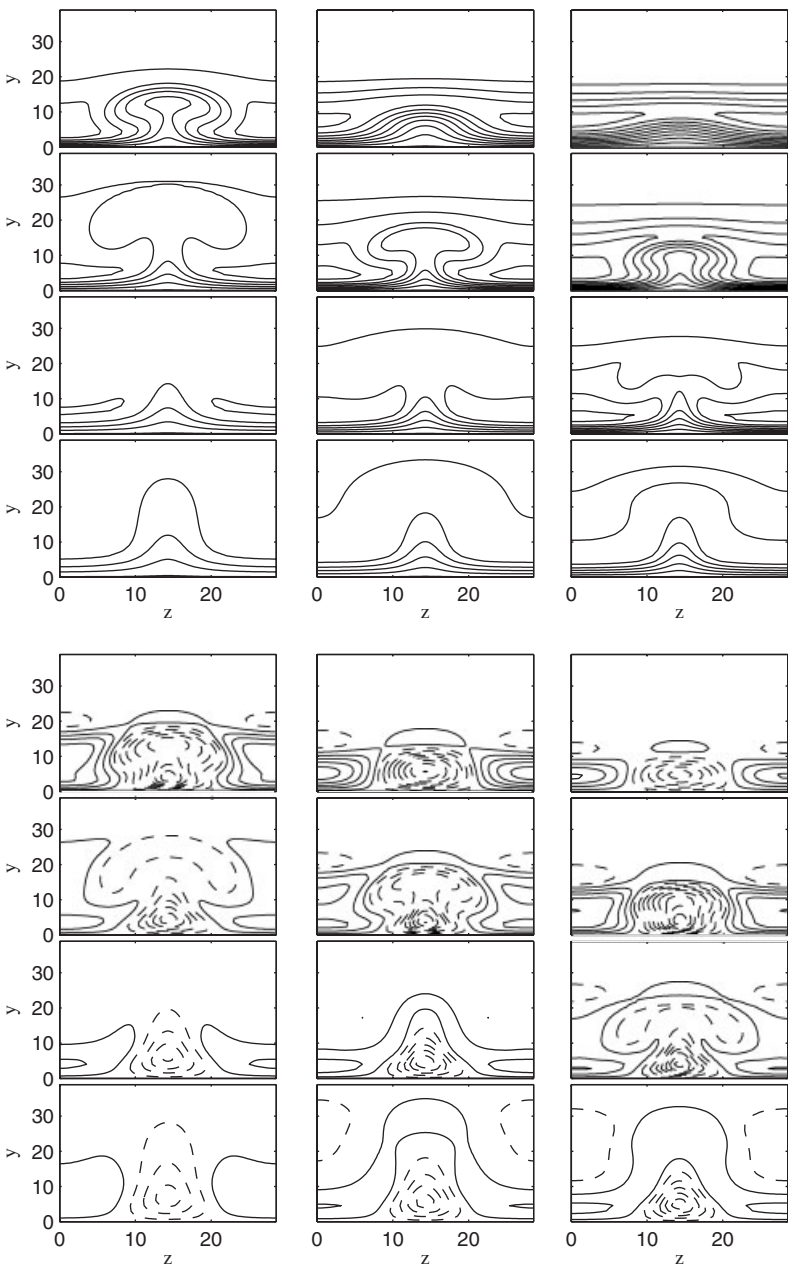

Figure 7. Streamwise velocity and disturbance velocity ($Go = 2$, $\alpha = 0.22$, concave wall, branch 2). Left column: $m = -0.4$, $f''(0) = 0.32$; middle column: $m = -0.4$, $f''(0) = 0.97$; right column: $m = -0.405$ ($x = 9$, 12, 15, and 18).

DOI: 10.1002/fld

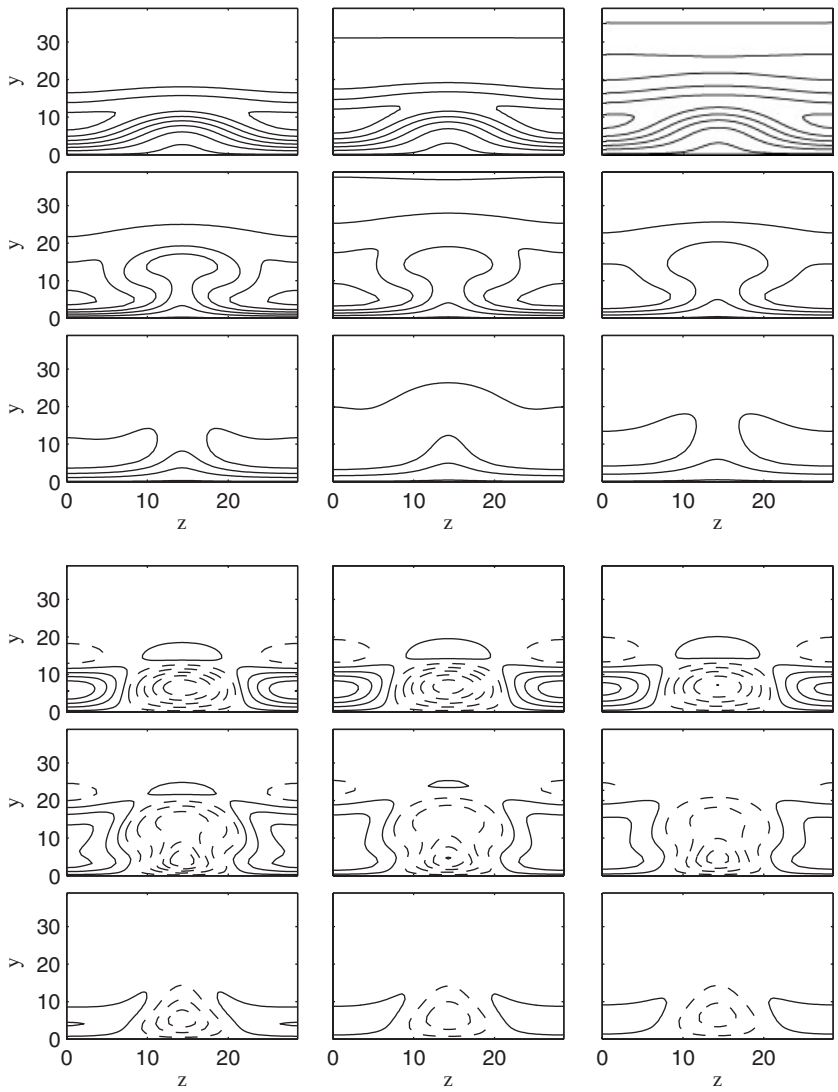

Figure 8. Streamwise velocity and disturbance velocity for $Go = 2$, $\alpha = 0.22$ on a concave wall. Left column ($m = -0.546$, branch 3), middle column ($m = -0.627$, branch 4), and right column ($m = -0.685$, branch 5). Streamwise positions $x = 6$, 9, and 12.

strength of vortices will be lower far downstream in the nonlinear region than for flows without overshoot.

In Figure 9, a comparison is shown between the flow on a concave (full line) and a convex wall (dashed line) for overshoot velocity profiles on branch 2 and $\alpha = 0.22$. It is clear that streamwise vortices are amplified on both types of walls. We found that for ($m = -0.4$, $f''(0) = 0.32$) on the concave wall, the flow is more unstable in the initial linear region than the flow without pressure

DOI: 10.1002/fld

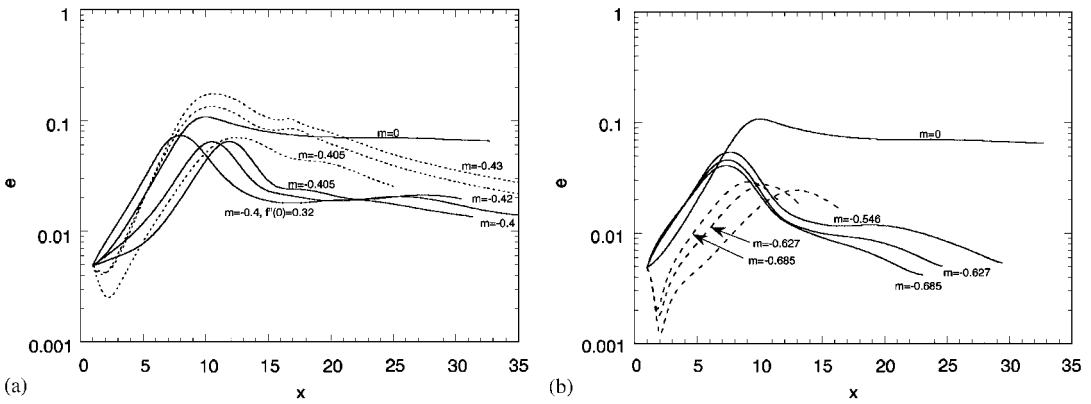

Figure 9. Streamwise development ($\alpha = 0.22$) of integrated disturbance velocity e in flows with velocity overshoot for different m. Full lines: concave curvature; dashed lines: convex curvature.

gradient. For all three pressure gradients shown on a concave wall, both the maximum amplitude and the saturation amplitude further downstream is lower than without pressure gradient. On the convex wall, the vortices decrease their amplitude near the starting streamwise position. However, further downstream streamwise vortices are also amplified on the convex wall ($m = -0.405$, -0.42 and -0.43 in Figure 9(a)) and the maximum integrated disturbance amplitude is larger for $m = -0.42$ and -0.43 than for the Blasius boundary layer ($m = 0$) on a concave wall. In Figure 9(b) a comparison is shown on curved walls along branches 3–5. For the concave flow in the linear region, the growth of vortices is almost the same independent of branch but a lower pressure gradient gives a lower maximum amplitude and a more rapid decay of the amplitude in the nonlinear region.

7. CONCLUDING REMARKS

This paper has shown nonlinear calculations of streamwise vortices in Falkner–Skan flows with self-similar suction or blowing on both concave and convex walls. Self-similar suction stabilize the Blasius boundary layer and blowing is destabilizing. The most unstable level of blowing is dependent on spanwise wave number. An adverse pressure gradient was found to destabilize the flow in the linear growth region but further downstream the strength of vortices was lower than without pressure gradient. Correspondingly, for a favourable pressure gradient the flow was stabilized in the linear region but more unstable in the nonlinear region. The combined effects of both a favourable pressure gradient and self-similar suction was found to stabilize the flow substantially compared with the single influence of suction or pressure gradient.

For adverse pressure gradients, the mean flow can theoretically have an overshoot in the streamwise velocity component. However, the overshoot velocity profiles for Falkner–Skan flows remain to be experimentally verified. They can be viewed as wall jet flow in a retarded outer flow. Such profiles in this paper have been shown to be unstable on both concave and convex walls. Generally, Görtler vortices related to overshoot profiles get a lower amplitude in the nonlinear region than velocity profiles without overshoot due to a very rapid decay of the outer flow related to low values

DOI: 10.1002/fld

of the pressure gradient. Moreover, Görtler vortices in overshoot velocity flows cannot, due to the shape of the velocity profile, grow out of the boundary layer as far away from the wall as for profiles without overshoot.

In this paper, the nonlinear development of streamwise vortices had been studied for multiple solutions of the Falkner–Skan equation. However, only the most fundamental branch of the Falkner–Skan equation without velocity overshoot has so far been experimentally verified and it is possible that most of the multiple solutions would be difficult to observe in a laboratory. Therefore, as a continuation of this paper, it would be important to use the present numerical method to study some new interesting solutions of boundary-layer equations as described by Liao and Magyari [30] and Liao [31].

APPENDIX

$$a_{1k}^{j+1}=a_{3k}^{j+1}=\frac{2}{\Delta\eta^2},\quad a_{2k}^{j+1}=\frac{-4}{\Delta\eta^2}-\frac{3(1-m)\xi_{j+1}f_{1k}}{2\Delta\xi} \tag{A1}$$

$$b_{1k}^{j+1}=-b_{3k}^{j+1}=\frac{-(1+m)f_k}{2\Delta\eta}+\frac{\gamma(1+m)}{\Delta\eta}$$

$$b_{2k}^{j+1}=-(1-m)\eta_k f_{2k}+2n^2\alpha^2\xi_{j+1}^2+2mf_{1k} \tag{A2}$$

$$b_{4k}^{j+1}=2\xi^{\frac{1+m}{1-m}}f_{2k},\quad b_{5k}^{j+1}=\frac{-2(1-m)\xi_{j+1}f_{1k}}{\Delta\xi},\quad b_{6k}^{j+1}=\frac{(1-m)\xi_{j+1}f_{1k}}{2\Delta\xi} \tag{A3}$$

$$c_{1k}^{j+1}=c_{5k}^{j+1}=\frac{4\xi_{j+1}}{\Delta\eta^4},\quad c_{2k}^{j+1}=c_{4k}^{j+1}=\frac{-16\xi_{j+1}}{\Delta\eta^4}-\frac{3(1-m)\xi_{j+1}^2f_{1k}}{\Delta\xi\Delta\eta^2} \tag{A4}$$

$$c_{3k}^{j+1}=\frac{24\xi_{j+1}}{\Delta\eta^4}+\frac{6(1-m)\xi_{j+1}^2f_{1k}}{\Delta\xi\Delta\eta^2}+\frac{3(1-m)(\xi_{j+1}^2f_{3k}+n^2\alpha^2\xi_{j+1}^4f_{1k}}{\Delta\xi} \tag{A5}$$

$$d_{1k}^{j+1}=-d_{5k}^{j+1}=\frac{-(1+m)\xi_{j+1}f_k}{\Delta\eta^3}+\frac{2\gamma\xi_{j+1}(1+m)}{\delta\eta^3} \tag{A6}$$

$$d_{2k}^{j+1}=\frac{2(1+m)\xi_{j+1}(f_k-2\gamma)}{\Delta\eta^3}+\frac{2(1-m)\xi_{j+1}\eta_k f_{2k}-4\xi_{j+1}f_{1k}+8n^2\alpha^2\xi_{j+1}^3}{\Delta\eta^2}$$
$$\times\frac{4(1-m)\xi_{j+1}\eta_k f_{3k}+2(1-3m)\xi_{j+1}f_{2k}+2(1+m)n^2\alpha^2\xi_{j+1}^3(f_k-2\gamma)}{2\Delta\eta} \tag{A7}$$

$$d_{3k}^{j+1}=2(1-m)\eta_k\xi_{j+1}f_{4k}+4(1-2m)\xi_{j+1}f_{3k}-2(1-m)\eta_k\xi_{j+1}^3n^2\alpha^2f_{2k}+4n^2\alpha^2\xi_{j+1}^3mf_{1k}$$
$$-4n^4\alpha^4\xi_{j+1}^5-\frac{4(1-m)\xi_{j+1}\eta_k f_{2k}-8\xi_{j+1}f_{1k}+16n^2\alpha^2\xi_{j+1}^3}{\Delta\eta^2} \tag{A8}$$

DOI: 10.1002/fld

$$d_{4k}^{j+1} = \frac{-2(1+m)\xi_{j+1}(f_k - 2\gamma)}{\Delta\eta^3} + \frac{2(1-m)\xi_{j+1}\eta_k f_{2k} - 4\xi_{j+1} f_{1k} + 8n^2\alpha^2\xi_{j+1}^3}{\Delta\eta^2}$$
$$- \frac{4(1-m)\xi_{j+1}\eta_k f_{3k} + 2(1-3m)\xi_{j+1} f_{2k} + 2(1+m)n^2\alpha^2\xi_{j+1}^3(f_k + 2\gamma)}{2\Delta\eta} \tag{A9}$$

$$d_{6k}^{j+1} = -\frac{\xi^{2m/(m-1)}[2(1-3m+2m^2)\eta_k f_{2k} + (1-2m+m^2)\eta_k^2 f_{3k} + 2m(m-1) f_{1k}]}{\Delta\eta}$$
$$+ \frac{3\xi^{(3m-1)/(m-1)}[(1-2m+m^2)\eta_k f_{2k} - m(1-m) f_{1k}]}{2\Delta\xi\Delta\eta}$$
$$- \frac{\xi^{2m/(m-1)}[(1-m^2)(f_k - \eta_k f_{1k}) + (1-2m+m^2)\eta_k^2 f_{2k} - 2\gamma(1-m^2)]}{\Delta\eta^2} \tag{A10}$$

$$d_{7k}^{j+1} = -\xi^{2m/(m-1)}[(1-2m+m^2)\eta_k^2 f_{4k} + (5-12m+7m^2)\eta_k f_{3k} + 3(1-4m+3m^2) f_{2k}]$$
$$- n^2\alpha^2\xi^{(4m-2)/(m-1)}[(1-m^2)(f_k - 2\gamma) - (1-4m+3m^2)\eta_k f_{1k} - (1-2m+m^2)\eta_k^2 f_{2k}]$$
$$+ 8(-1)^q n^2\alpha^2 G^2\xi^{(3m-5)/(m-1)}(f_{1k})$$
$$+ \frac{3\xi^{(3m-1)/(m-1)}[(1-2m+m^2)\eta_k f_{3k} + (1-4m+3m^2) f_{2k}]}{\Delta\xi}$$
$$+ \frac{2\xi^{2m/(m-1)}[(1-2m+m^2)\eta_k^2 f_{2k} + (1-m^2)(f_k - \eta_k f_{1k} - 2\gamma)]}{\Delta\eta^2} \tag{A11}$$

$$d_{8k}^{j+1} = \frac{\xi^{2m/(m-1)}[2(1-3m+2m^2)\eta_k f_{2k} + (1-2m+m^2)\eta_k^2 f_{3k} + 2m(m-1) f_{1k}]}{\Delta\eta}$$
$$- \frac{3\xi^{(3m-1)/(m-1)}[(1-2m+m^2)\eta_k f_{2k} - m(1-m) f_{1k}]}{2\Delta\xi\Delta\eta}$$
$$- \frac{\xi^{2m/(m-1)}[(1-m^2)(f_k - \eta_k f_{1k}) + (1-2m+m^2)\eta_k^2 f_{2k} - 2\gamma(1-m^2)]}{\Delta\eta^2} \tag{A12}$$

$$d_{9k}^{j+1} = -d_{11k}^{j+1} = \frac{-2\xi^{(3m-1)/(m-1)}[(1-m)^2\eta_k f_{2k} - 2m(1-m) f_{1k}]}{\Delta\xi\Delta\eta} \tag{A13}$$

$$d_{10k}^{j+1} = \frac{-4\xi^{(3m-1)/(m-1)}[(1-m)^2\eta_k f_{3k} + (1-4m+3m^2) f_{2k}]}{\Delta\xi} \tag{A14}$$

$$d_{12k}^{j+1} = d_{14k}^{j+1} = \frac{-4\xi^2(1-m) f_{1k}}{\Delta\xi\Delta\eta^2}$$

DOI: 10.1002/fld

$$d_{13k}^{j+1} = \frac{8\xi^2(1-m)f_{1k}}{\Delta\xi\Delta\eta^2} + \frac{4\xi^2(1-m)(f_{3k}+n^2\alpha^2\xi^2 f_{1k})}{\Delta\xi} \tag{A15}$$

$$d_{15k}^{j+1} = d_{17k}^{j+1} = \frac{\xi^2(1-m)f_{1k}}{\Delta\xi\Delta\eta^2}$$

$$d_{16k}^{j+1} = \frac{-2\xi^2(1-m)f_{1k}}{\Delta\xi\Delta\eta^2} - \frac{\xi^2(1-m)(f_{3k}+n^2\alpha^2\xi^2 f_{1k})}{\Delta\xi} \tag{A16}$$

$$d_{18k}^{j+1} = -d_{20k}^{j+1} = \frac{\xi^{(3m-1)/(m-1)}[(1-m)^2\eta_k f_{2k} - 2m(1-m)f_{1k}]}{2\Delta\xi\Delta\eta} \tag{A17}$$

$$d_{19k}^{j+1} = \frac{\xi^{(3m-1)/(m-1)}[(1-m)^2\eta_k f_{3k} + (1-4m+3m^2)f_{2k}]}{\Delta\xi} \tag{A18}$$

$$g_{1k}^{j+1} = -2\mathrm{i}n\alpha\xi^{2/(1-m)}, \quad h_{1k}^{j+1} = -h_{3k}^{j+1} = \frac{(m-1)\eta_k}{2\Delta\eta}$$

$$h_{5k}^{j+1} = \frac{-h_{4k}^{j+1}}{4} = \frac{h_{2k}^{j+1}}{3} = \frac{(1-m)\xi_{j+1}}{2\Delta\xi} \tag{A19}$$

$$h_{6k}^{j+1} = -h_{7k}^{j+1} = \frac{\xi_{j+1}^{(1+m)/(1-m)}}{2\Delta\eta} \tag{A20}$$

ACKNOWLEDGEMENTS

Thanks are due to Dr Benmalek and Prof. Saric for letting me use and modify their code.

REFERENCES

1. Rosenhead L. *Laminar Boundary Layers*. Oxford University Press: Oxford, 1963.
2. Libby PA, Liu TM. Further solutions of the Falkner–Skan equation. *AIAA Journal* 1967; **5**:1040–1042.
3. Steinheuer J. Similar solutions of the laminar wall jet in a decelerating outer flow. *AIAA Journal* 1967; **6**: 1040–1042.
4. Glauert MB. The wall jet. *Journal of Fluid Mechanics* 1956; **1**:625–632.
5. Zaturska MB, Banks WHH. A new solution branch of the Falkner–Skan equation. *Acta Mechanica* 2001; **152**:197–201.
6. White FM. *Viscous Fluid Flow* (3rd edn). McGraw-Hill: New York, 2006.
7. Sobey IJ. *Introduction to Interactive Boundary Layer Theory*. Oxford University Press: Oxford, 2000.
8. Hall P. Görtler vortices in growing boundary layers: the leading edge receptivity problem, linear growth and the nonlinear breakdown stage. *Mathematika* 1990; **37**:151–189.
9. Saric WS. Görtler vortices. *Annual Review of Fluid Mechanics* 1994; **26**:379–409.
10. Floryan JM. On the Görtler instability of boundary layers. *Progress in Aerospace Sciences* 1991; **28**:235–271.
11. Kahawita RA. Instability of laminar wall jets along curved surfaces. *AIAA Journal* 1991; **13**:1517–1518.
12. Floryan JM. Görtler instability of boundary layers over concave and convex walls. *Physics of Fluids* 1986; **29**:2380–2387.

DOI: 10.1002/fld

13. Floryan JM. Görtler instability of wall jets. *AIAA Journal* 1989; **27**:112–114.
14. Matsson OJE. On the curved wall jet influenced by system rotation and self similar suction or blowing. *Physics of Fluids* 1995; **7**:3048–3059.
15. Wadey PD. On the development of Görtler vortices in wall jet flow. *Journal of Engineering Mathematics* 1992; **26**:297–313.
16. Matsson OJE. Experiments on streamwise vortices in curved wall jet flow. *Physics of Fluids* 1995; **7**:2978–2988.
17. Le Cunff C, Zebib A. Nonlinear spatially developing Görtler vortices in curved wall jet flow. *Physics of Fluids* 1996; **8**:2375–2384.
18. Matsson OJE. Görtler vortices in wall jet flow on a rotating cylinder. *Physics of Fluids* 1998; **10**:2238–2248.
19. Ragab SA, Nayfeh AH. Görtler instability. *Physics of Fluids* 1981; **24**:1405–1417.
20. Goulpie P, Klingmann BGB, Bottaro A. Görtler vortices in boundary layers with streamwise pressure gradient: linear theory. *Physics of Fluids* 1996; **8**:451–459.
21. Itoh N. A non-parallel theory for Görtler instability of Falkner–Skan boundary layers. *Fluid Dynamics Research* 2001; **28**:383–396.
22. Aihara Y, Sonoda T. Effects of pressure gradient on the secondary instability of Görtler vortices. *AIAA-81-0197*.
23. Floryan JM, Saric WS. Effects of suction on the Görtler instability of boundary layers. *AIAA Journal* 1983; **21**:1635–1639.
24. Floryan JM. Effects of blowing on the Görtler instability of boundary layers. *AIAA Journal* 1985 **23**:1287–1288.
25. Lin MH, Hwang GJ. Numerical prediction of the formation of Goertler vortices on a concave surface with suction and blowing. *International Journal for Numerical Methods in Fluids* 1999; **31**:1281–1295.
26. Myose RY, Blackwelder RF. Control of streamwise vortices using selective suction. *AIAA Journal* 1995; **33**: 1076–1080.
27. Benmalek A. Nonlinear development of Görtler vortices over variable curvature walls. *Ph.D. Thesis*, Arizona State University, Tempe, AZ, 1993.
28. Benmalek A, Saric WS. Effects of curvature variations on the nonlinear evolution of Goertler vortices. *Physics of Fluids* 1994; **6**:3353–3367.
29. Liao S. A non-iterative numerical approach for two-dimensional viscous flow problems governed by the Falkner–Skan equation. *International Journal for Numerical Methods in Fluids* 2001; **35**:495–518.
30. Liao SJ, Magyari E. Exponentially decaying boundary layers as limiting cases of families of algebraically decaying ones. *Zeitschrift fur Angewandte Mathematik und Physik* 2006; **57**:777–792.
31. Liao SJ. A new branch of solutions of boundary-layer flows over an impermeable stretched plate. *International Journal of Heat and Mass Transfer* 2005; **48**:2529–2539.

DOI: 10.1002/fld